The Astrophysical Journal, 695:1227–1232, 2009 April 20 doi:10.1088/0004-637X/695/2/1227

DISCOVERY OF THE MOST DISTANT DOUBLE-PEAKED EMITTER AT $z = 1.369$

B. Luo[1], W. N. Brandt[1], J. D. Silverman[2], I. V. Strateva[3], F. E. Bauer[4], P. Capak[5], J. Kartaltepe[6], B. D. Lehmer[7], V. Mainieri[8], M. Salvato[5], G. Szokoly[9,3], D. P. Schneider[1], and C. Vignali[10]
[1] Department of Astronomy & Astrophysics, 525 Davey Lab, The Pennsylvania State University, University Park, PA 16802, USA
[2] Institute of Astronomy, ETH Zurich, 8092, Zurich, Switzerland
[3] Max Planck Institute for Extraterrestrial Physics, Garching, 85741, Germany
[4] Columbia Astrophysics Laboratory, Columbia University, Pupin Laboratories, 550 West 120th Street, New York, NY 10027, USA
[5] California Institute of Technology, 1200 East California Boulevard, Pasadena, CA 91125, USA
[6] Institute for Astronomy, University of Hawaii, 2680 Woodlawn Drive, Honolulu, HI 96822, USA
[7] Department of Physics, Durham University, Durham DH1 3LE, UK
[8] European Southern Observatory, Karl-Schwarzschild-Strasse 2, Garching, D-85748, Germany
[9] Eötvös University, Institute of Physics, 1117 Budapest, Pázmány P. s. 1/A, Hungary
[10] Universitá di Bologna, Via Ranzani 1, Bologna, Italy
Received 2008 October 20; accepted 2009 January 19; published 2009 April 7

ABSTRACT

We report the discovery of the most distant double-peaked emitter, CXOECDFS J033115.0–275518, at $z = 1.369$. A Keck/DEIMOS spectrum shows a clearly double-peaked broad Mg II λ2799 emission line, with FWHM ≈ 11,000 km s^{-1} for the line complex. The line profile can be well fitted by an elliptical relativistic Keplerian disk model. This is one of a handful of double-peaked emitters known to be a luminous quasar, with excellent multiwavelength coverage and a high-quality X-ray spectrum. CXOECDFS J033115.0–275518 is a radio-loud quasar with two radio lobes (FR II morphology) and a radio loudness of $f_{5\,\mathrm{GHz}}/f_{4400\,\text{Å}} \approx 429$. The X-ray spectrum can be modeled by a power law with photon index 1.72 and no intrinsic absorption; the rest-frame 0.5–8.0 keV luminosity is 5.0×10^{44} erg s^{-1}. The spectral energy distribution (SED) of CXOECDFS J033115.0–275518 has a shape typical for radio-loud quasars and double-peaked emitters at lower redshift. The local viscous energy released from the line-emitting region of the accretion disk is probably insufficient to power the observed line flux, and external illumination of the disk appears to be required. The presence of a big blue bump in the SED along with the unexceptional X-ray spectrum suggest that the illumination cannot arise from a radiatively inefficient accretion flow.

Key words: accretion, accretion disks – galaxies: active – galaxies: nuclei – line: profiles – quasars: emission lines

1. INTRODUCTION

Double-peaked emitters are active galactic nuclei (AGNs) emitting broad and double-peaked low-ionization lines. A survey of ∼100 radio-loud AGNs ($z < 0.4$) suggests that ∼20% of these sources are double-peaked emitters (Eracleous & Halpern 1994, 2003). The frequency of double-peaked emitters is much lower (∼3%) among the general population of ∼3000 low-redshift ($z < 0.33$) AGNs selected by the Sloan Digital Sky Survey (Strateva et al. 2003), and these double-peaked emitters are predominantly (76%) radio quiet. Since the discovery of the first examples of double-peaked emitters in the 1980s (Oke 1987; Chen et al. 1989), more than 150 such sources have been found. Most have been identified based on their Hα, and sometimes Hβ, lines. Spectroscopy of several of these sources showed that the Mg II λ2799 line[11] also has a double-peaked profile similar to those of Hα and Hβ (Halpern et al. 1996; Eracleous et al. 2004). Selection based on the Mg II line profile could in principle find higher redshift candidates; however, due to contamination from the underlying Fe II and Fe III emission-line complexes (e.g., Wills et al. 1985) and possibly Mg II self-absorption, it is difficult to create a complete sample of double-peaked Mg II λ2799 emitters, and only a few such objects have been reported (Strateva et al. 2003). The highest redshift double-peaked emitters discovered to date have $z \approx 0.6$.

Observational results and basic physical considerations indicate that the most plausible origin of the double-peaked emission lines is the accretion disk (e.g., Chen & Halpern 1989; Eracleous et al. 1995; Eracleous & Halpern 2003). The line profile can be well fitted by emission from the outer regions of a Keplerian disk, typically at distances from the black hole of hundreds to thousands of gravitational radii ($R_G = GM/c^2$). In many cases, the viscous energy available locally in the line-emitting region is insufficient to power the observed lines, and it has been suggested that these strong lines are produced by external illumination of the disk, probably from an X-ray emitting elevated structure in the center (e.g., Chen et al. 1989).

In this paper, we report the discovery of the highest redshift double-peaked emitter known to date. This source, CXOECDFS J033115.0–275518 (hereafter J0331–2755), was detected as an X-ray point source in the ≈250 ks observations of the Extended *Chandra* Deep Field-South (E-CDF-S; Lehmer et al. 2005), and was identified as a double-peaked Mg II emitter at $z = 1.369$ by Keck/DEIMOS optical spectroscopy. We adopt a cosmology with $H_0 = 70$ km s^{-1} Mpc^{-1}, $\Omega_M = 0.3$, and $\Omega_\Lambda = 0.7$ throughout this paper.

2. KECK OBSERVATIONS AND DISK-MODEL FIT

Optical spectroscopic observations of J0331–2755 were carried out using the DEIMOS spectrograph (Faber et al. 2003) on the 10 m Keck II telescope on 2007 January 15 (UT), as part of the E-CDF-S spectroscopic program (P.I.s: P. Capak, M. Salvato, and J. Kartaltepe; D. Silverman et al. 2009, in preparation). We used the 600 l mm^{-1} grism and the

[11] This Mg II line is actually a λ2796/2803 doublet. Due to line broadening, the two components are usually blended and cannot be resolved. Thus, we treat the doublet as a single line when discussing the observed emission feature throughout this paper.

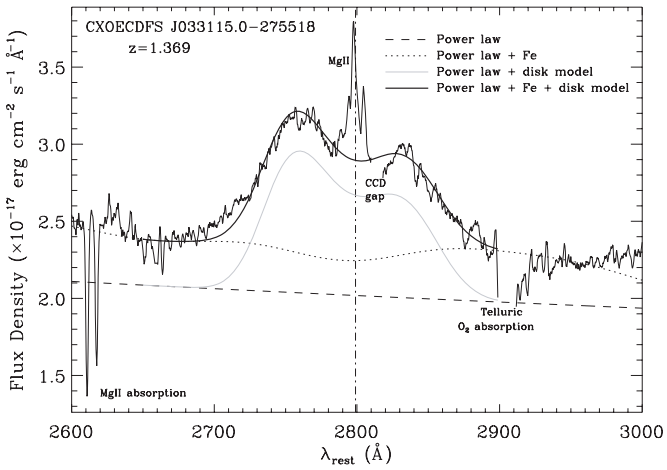

Figure 1. Rest-frame NUV spectrum of J0331–2755 showing the double-peaked Mg II line. The vertical dash-dotted line indicates the expected position of Mg II λ2799. Two gaps in the spectrum are caused by the DEIMOS CCDs and telluric O_2 absorption. Dashed, dotted, gray, and thick curves are different emission components used to fit the observed double-peaked Mg II line profile, as indicated in the plot. The rms noise of the spectrum is 1.3×10^{-18} erg cm^{-2} s^{-1} Å^{-1}.

GG455 filter. The wavelength coverage was ∼4650–8580 Å with a resolution of 3.5 Å. The seeing was 0.″6, and the air mass was 1.49. The total exposure time was 9000 s in five individual exposures. The wavelength-dependent response was corrected by an observation of a single flux standard star while the overall normalization was set to match the COMBO-17 *R*-band magnitude (Wolf et al. 2004, 2008). The redshift of J0331–2755, 1.369, was determined using the Mg II λ2799 and Ne V λ3426 narrow lines (FWHM ≈ 400 km s^{-1}).

The rest-frame near-UV (NUV) spectrum around the Mg II λ2799 line is shown in Figure 1, smoothed to a resolution of 3.6 Å. The spectrum shows a clearly double-peaked broad Mg II line along with a central narrow line, similar to previously discovered double-peaked Hα or Mg II emitters. The Mg II absorption doublet at ∼2600 Å is likely produced by an intervening absorber at $z = 1.21$, as inferred from the narrow velocity dispersion (FWHM ≈ 300 km s^{-1}) and large blueshift (e.g., Ganguly et al. 2007). An alternative interpretation of the doublet as arising in an AGN outflow would require outflow velocities of ∼20,000 km s^{-1}.

Assuming that the J0331–2755 Mg II line emission originates from the accretion disk, we can use the line shape to determine a set of parameters characterizing the emission region (see Chen & Halpern 1989; Eracleous et al. 1995, for a description of line-profile accretion-disk modeling). We start by subtracting the underlying continuum and Fe emission-line complexes, as shown in Figure 1. The continuum is represented by a simple power law, $F_\lambda \propto \lambda^{-1.6}$ (Vanden Berk et al. 2001). The Fe pseudocontinuum is modeled by the broadened Fe-emission template of Vestergaard & Wilkes (2001), fit to the ∼2450–2900 Å spectrum excluding the Mg II line, where we assumed that the Fe-line broadening is similar to that of the Mg II line complex, FWHM ≈ 11, 000 km s^{-1}. Such Fe-line broadening could result if the line is emitted from the base of a wind launched from the accretion disk. The double-peaked Mg II line profile does not differ much for any reasonable choice of the Fe-line broadening (from 5000 to 15,000 km s^{-1}).

The continuum and Fe line complex subtracted Mg II profile of J0331–2755 cannot be well fitted by a circular relativistic Keplerian disk model. In the absence of line-profile variability, which can help distinguish between the different nonaxisymmetric disk models, we choose the elliptical disk model of Eracleous et al. (1995), which has the smallest number of extra free parameters (for a total of seven disk-fit parameters). The model assumes an external source of illumination represented by a power law with emissivity, $\epsilon \propto R^{-q}$, and we fix $q = 3$, equivalent to an illuminating point source on the disk axis high above the disk. The central narrow-line part of the spectrum was excluded from the fit. From the best-fit model, the disk inclination with respect to our line of sight is $i = 22^{+8}_{-3}{}^\circ$, the inner and outer radii of the emission ring are $R_1 = 200^{+200}_{-50}\ R_G$ and $R_2 = 900^{+600}_{-100}\ R_G$, the turbulent broadening parameter is $\sigma = 1900^{+400}_{-200}$ km s^{-1}, and the disk ellipticity is $e = 0.4^{+0.1}_{-0.2}$, with a semimajor axis orientation of $\phi_0 = 110^\circ \pm 20^\circ$ with respect to our line of sight. The integrated line flux is $F_{\rm Mg\,II} = (9.3 \pm 0.2) \times 10^{-16}$ erg cm^{-2} s^{-1}. These emission-line region parameters are similar to those obtained for lower-redshift double-peaked emitters, e.g., Eracleous & Halpern (2003), Strateva et al. (2003), and Strateva et al. (2008).

3. MULTIWAVELENGTH PROPERTIES

The numerous multiwavelength deep surveys of the E-CDF-S allow us to study the properties of J0331–2755 from radio to X-ray wavelengths. Figure 2 presents the radio, infrared (IR), optical, and X-ray images of J0331–2755. A broadband spectral energy distribution (SED) of the source is shown in Figure 3, with the majority of the SED data displayed in Table 1. It is one of the best-sampled double-peaked emitter SEDs, comparable to that of the prototype source Arp 102B (Eracleous et al. 2003; Strateva et al. 2008). Details of the broadband properties are discussed below.

Radio. J0331–2755 was observed by the Very Large Array (VLA) at 1.4 GHz in 1999–2000 (Kellermann et al. 2008) and 2007 (Miller et al. 2008).[12] The reported core radio flux densities are 1.14 ± 0.03 and 1.23 ± 0.02 mJy, respectively. It was also detected by the Australia Telescope Compact Array (ATCA) at 1.4 GHz, with a ∼30% higher flux density (Rovilos et al. 2007). Because of the low resolution (beam size 17″ × 7″), we do not use the ATCA results. The average VLA flux density is plotted in Figure 3. We show the radio image from Miller et al. (2008) in Figure 2(a). Most of the data were obtained when the VLA was in configuration A, and some were obtained in configuration BnA. The beam size is 2.″8 × 1.″6 with a position angle near zero (i.e., N-S). The source is associated with two brighter radio lobes, which extend to a few hundred kpc away from the center, displaying an FR II morphology. The core and the lobes are sources 20, 19, and 21 in the catalog of Miller et al. (2008), and the total radio power at 1.4 GHz is $\sim 1.5 \times 10^{33}$ erg s^{-1} Hz^{-1}. According to the radio contours, there could also be a weak jet leading to the lobe in the western feature. We did not find any clear counterparts for the lobes/jet at other wavelengths, except for a faint optical source at the position of the eastern lobe. Moreover, these structures are more extended than nearby point sources. Thus, they are not likely physically associated with galaxies. The radio loudness parameter, defined as $R = f_{5\,\rm GHz}/f_{4400\,\text{Å}}$ (the ratio of flux densities in the rest frame; e.g., Kellermann et al. 1989), is computed using the 1.4 GHz and 914 nm COMBO-17 (Wolf et al. 2004, 2008) flux densities with the assumption of a radio power-law slope of $\alpha_r = -0.8$ and an

[12] http://taltos.pha.jhu.edu/∼nmiller/vlaecdfs_main.html.

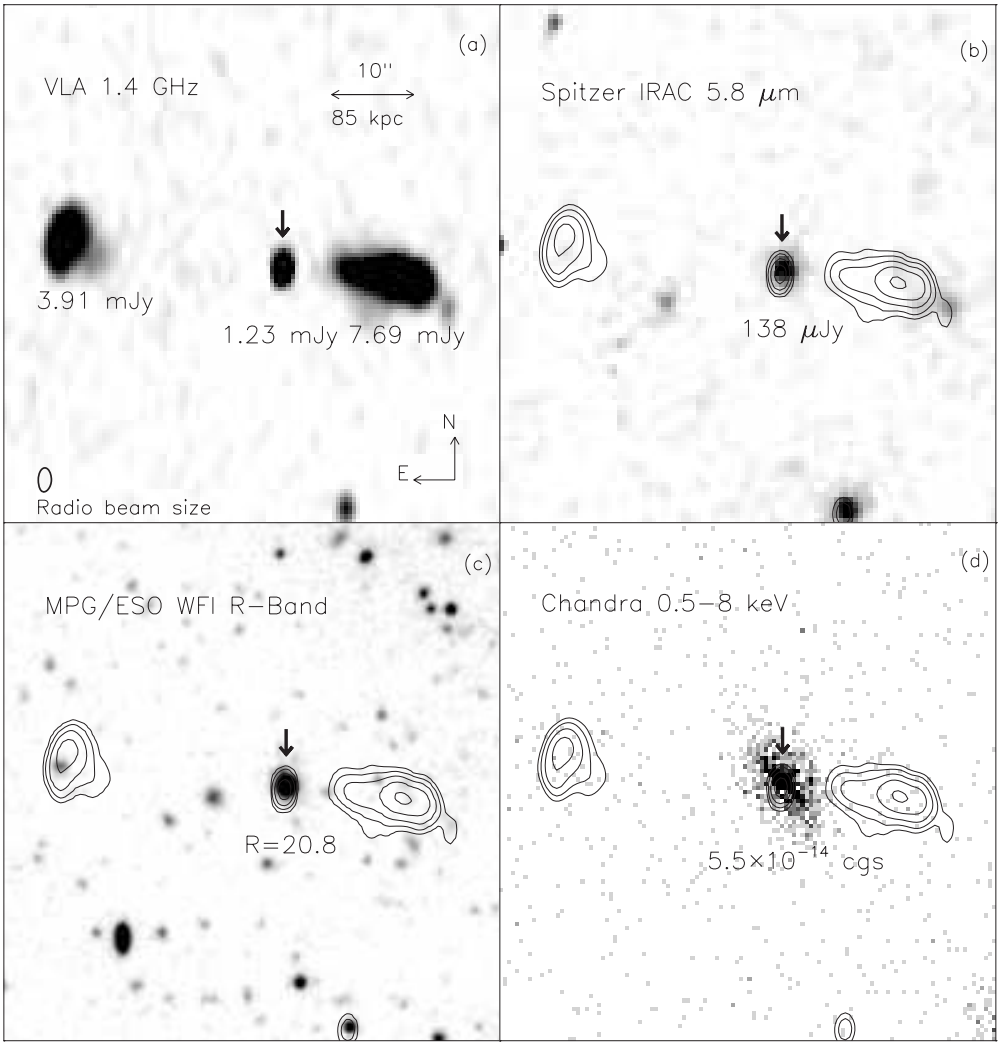

Figure 2. (*a*) Radio 1.4 GHz, (*b*) IR 5.8 μm, (*c*) optical *R*-band, and (*d*) X-ray 0.5–8 keV images of J0331–2755. Each image is 60″ (0.51 Mpc at z=1.369) on a side. The last three images are overlaid with radio contours, ranging from ≈ 0.6% to 90% of the maximum pixel value following a logarithmic scale. The downward arrows point to the position of J0331–2755. The ellipse at the lower left corner of (*a*) shows the beam size of the radio observations. Flux density or flux in each band is indicated; the X-ray flux is in units of erg cm^{-2} s^{-1}. The apparent extension in the *Chandra* image is due to the large point-spread function at its location.

optical power-law slope of $\alpha_o = -0.4$ ($F_\nu \propto \nu^\alpha$). The source has a radio loudness of $R \approx 429$, including the contributions from the extended lobe emission.[13]

IR. The E-CDF-S was covered by the *Spitzer* Far Infrared Deep Extragalactic Legacy Survey (FIDEL) at 24 and 70 μm,[14] and by the *Spitzer* IRAC/MUSYC Public Legacy Survey in the E-CDF-S (SIMPLE) at 3.6, 4.5, 5.8, and 8.0 μm.[15] J0331–2755 was detected at 3.6, 4.5, 5.8, 8.0, and 24 μm with flux densities of 0.09, 0.12, 0.14, 0.19, and 0.50 mJy, respectively (e.g., see Figure 2(b)). It was not detected at 70 μm; we estimate the 2σ flux-density upper limit to be 1.5 mJy.

Optical, UV. In the optical band, J0331–2755 is present in the COMBO-17 catalog (Wolf et al. 2004, 2008) and the deep MPG/ESO Wide Field Imager (WFI) *R*-band catalog (Giavalisco et al. 2004). It is outside the field of view of the Galaxy Evolution from Morphologies and SEDs (GEMS) survey (Caldwell et al. 2008). The *B*-band absolute AB magnitude is $M_B = -23.4$. The WFI *R*-band image is shown in Figure 2(c) and the 17-band photometry data points from the COMBO-17 observations are shown in Figure 3. The Galactic extinction in the optical band is small (a correction factor of ∼1.02 for the *V* band). J0331–2755 was observed by *Galaxy Evolution Explorer* (*GALEX)* in 2003 and 2005.[16] The observed NUV ($\lambda_{\rm eff} = 2267$ Å) flux densities are 5.95 ± 0.13 and 7.69 ± 0.23 μJy, brightening by ∼30% in two years. This variability amplitude is typical for double-peaked emitters (e.g., Gezari et al. 2007; Strateva et al. 2008). The correction factor for the NUV Galactic extinction is ∼1.07, following the Galactic extinction law of $A_{\rm NUV} = 8.0E(B-V)$ (e.g., Gil de Paz et al. 2007). The source was not detected in the far-UV band ($\lambda_{\rm eff} = 1516$ Å), due to the Lyman break at rest-frame 912 Å. The average NUV flux density is shown in Figure 3.

X-ray. J0331–2755 was detected during the *Chandra* E-CDF-S survey in 2004, with an effective exposure time of ≈210 ks. It is located at the edge of the E-CDF-S field and has an off-axis angle of ∼8′. The *Chandra* image is

[13] The integrated radio flux density was used to compute the radio loudness in order to be consistent with the typical definition in the literature. The radio loudness is ∼41 if only the radio flux from the core component is taken into account.

[14] See http://ssc.spitzer.caltech.edu/legacy/fidelhistory.html.

[15] See http://ssc.spitzer.caltech.edu/legacy/simplehistory.html.

[16] See http://galex.stsci.edu/GR4/.

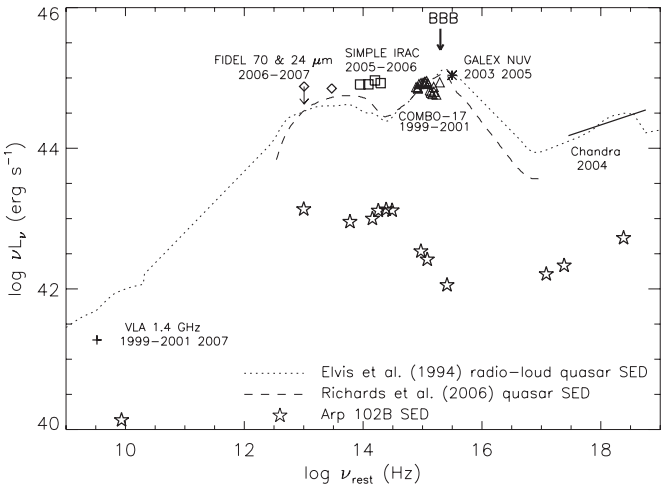

Figure 3. Radio through X-ray SED of J0331–2755. The names of observatories/surveys and years of observations are indicated for the data points. The dotted and dashed curves show the Elvis et al. (1994) and Richards et al. (2006) SED templates, normalized to the COMBO-17 *R*-band data point, respectively. The SED of J0331–2755 is in general agreement with typical radio-loud quasar SEDs. The Arp 102B SED (Eracleous et al. 2003; Strateva et al. 2008, and references therein) is also shown for comparison. The J0331–2755 SED and both of the SED templates show a BBB in the UV (marked with a thick downward-pointing arrow), while the Arp 102B SED does not.

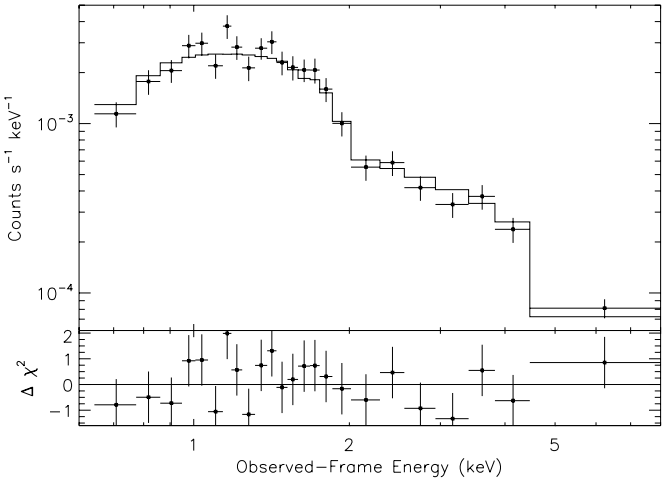

Figure 4. X-ray spectrum of J0331–2755 overlaid with the best-fit model. The bottom panel shows the deviation of the data from the model in units of σ, with error bars of size unity. The spectrum can be modeled with a simple power law modified by Galactic absorption; the best-fit photon index for this model is $\Gamma = 1.72 \pm 0.10$.

shown in Figure 2(d). J0331–2755 has one of the best X-ray spectra available for double-peaked emitters; the number of 0.5–8.0 keV source counts is 1048. We performed spectrum extraction on the reduced and cleaned level 2 event files (Lehmer et al. 2005) using the reduction tool ACIS EXTRACT (AE; Broos et al. 2000). The spectrum was binned at a signal-to-noise ratio of 5 using AE and then fit with XSPEC (ver. 12.4.0; Arnaud 1996). The 0.5–8.0 keV spectrum can be well modeled with a power law modified by Galactic absorption, with $\chi^2 = 18.0$ for 22 degrees of freedom (see Figure 4). We adopted a Galactic neutral hydrogen column density $N_{\rm H,G} = 8.8 \times 10^{19}$ cm^{-2} (Stark et al. 1992). The best-fit photon index is $\Gamma = 1.72 \pm 0.10$; the uncertainties are quoted at 90% confidence. This photon index is typical for radio-loud quasars, $\Gamma_{\rm RL} \approx 1.6$–$1.7$ (e.g., Reeves et al. 1997). The rest-frame unabsorbed 0.5–8.0 keV luminosity is 5.0×10^{44} erg s^{-1}, well within the quasar regime. Intrinsic absorption ($N_{\rm H,i}$ at $z = 1.369$) is not required to fit the spectrum, with a 90% confidence upper limit of 1.09×10^{22} cm^{-2}.

To compare the SED of J0331–2755 to those for typical quasars, we show in Figure 3 the mean quasar SED from Richards et al. (2006) and the mean radio-loud quasar SED from Elvis et al. (1994), both normalized to the COMBO-17 *R*-band flux of J0331–2755. The Richards et al. (2006) SED template is derived from a sample of radio-quiet sources, and does not cover the radio and X-ray bands. The optical-to-X-ray data agree reasonably well with the mean quasar SEDs. The excess emission in the IR bands suggests a contribution from the host galaxy, similar to some other double-peaked emitters (e.g., Strateva et al. 2008). The weaker radio emission than the mean radio-loud SED probably arises because we only include the radio emission from the core, while some of the Elvis et al. (1994) objects included extended radio emission when only low-resolution observations were available. As the multiwavelength data were not taken simultaneously, variations in the fluxes at different wavebands are likely responsible for part of the discrepancies between the data and SED templates. Thus the broadband SED of J0331–2755 does not differ significantly from those of typical radio-loud quasars, despite the double-peaked nature of this source. The bolometric luminosity estimated based on the Elvis et al. (1994) template is $L_{\rm bol} \approx 5.7 \times 10^{45}$ erg s^{-1}, corresponding to an accretion rate of $\sim 1\ M_\odot$ yr^{-1} under the assumption of accretion efficiency $\eta = 0.1$. Note that the template SED will "double-count" the IR emission if the IR bump consists of reprocessed nuclear continuum emission, which could result in an overestimate of the bolometric luminosity by up to 20%–30%.

4. DISCUSSION

The discovery of J0331–2755 doubles the redshift range of known double-peaked emitters, from ~0.6 to 1.369. The rest-frame 2500 Å monochromatic luminosity of J0331–2755 is 7.2×10^{29} erg s^{-1} Hz^{-1}, interpolated from the COMBO-17 flux densities. It is thus among the few most optically luminous double-peaked emitters known. Figure 5 shows the position of J0331–2755 in the redshift versus 2500 Å monochromatic luminosity plane. Data for the other double-peaked emitters are from Strateva et al. (2008) and references therein. The X-ray and bolometric luminosities of J0331–2755 are also comparable to those for the brightest double-peaked emitters. The UV-to-X-ray index, defined as $\alpha_{\rm OX} = -0.3838 \log[F_\nu(2500\ {\rm Å})/F_\nu(2\ {\rm keV})]$, is -1.27. Compared to the $\alpha_{\rm OX}$–$L_{2500\ {\rm Å}}$ relation for typical radio-quiet AGNs in Steffen et al. (2006), J0331–2755 has a flatter $\alpha_{\rm OX}$ (predicted $\alpha_{\rm OX} = -1.45$ at this $L_{2500\ {\rm Å}}$). This factor of ~3 X-ray enhancement is expected given the radio-loud nature of the source; jet-linked X-ray emission is likely making a substantial contribution to the X-ray spectrum.

Following Eracleous & Halpern (1994), we estimated the viscous power released in the line-emitting region $W_{\rm d}$. Assuming an accretion efficiency of $\eta \approx 0.1$ ($L_{\rm bol} = \eta \dot{M} c^2$), the gravitational power output is given by

$$W_{\rm d} = 7.7 \times L_{\rm bol} \left[\frac{1}{\zeta_1} \left(1 - \sqrt{\frac{8}{3\zeta_1}} \right) - \frac{1}{\zeta_2} \left(1 - \sqrt{\frac{8}{3\zeta_2}} \right) \right] {\rm erg\ s^{-1}}, \quad (1)$$

where ζ_1 and ζ_2 are the inner and outer radii of the

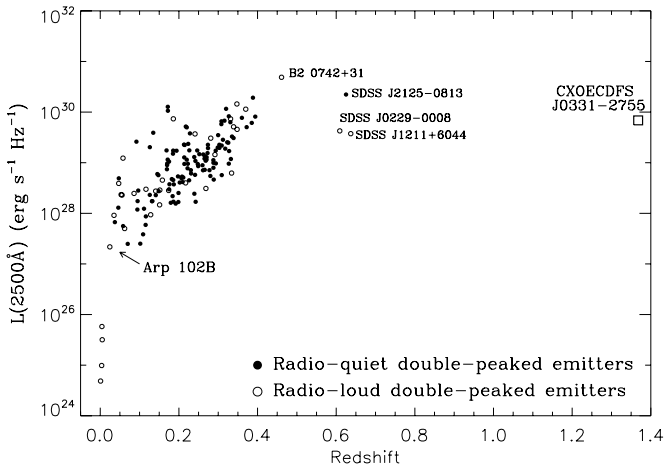

Figure 5. Redshift–luminosity distribution of double-peaked emitters (adapted from Strateva et al. 2008). Filled dots represent radio-quiet sources, and open dots represent radio-loud sources. The positions of J0331–2755, Arp 102B, and a few high-redshift sources are indicated.

Table 1
SED Data for J0331–2755

Band	log νL_ν (erg s^{-1})
Radio	
VLA 1.4 GHz	41.27
Infrared	
FIDEL 70 μm	<44.88
FIDEL 24 μm	44.85
SIMPLE 8.0 μm	44.91
SIMPLE 5.8 μm	44.91
SIMPLE 4.5 μm	44.96
SIMPLE 3.6 μm	44.93
Optical [a]	
COMBO-17 I	44.85
COMBO-17 R	44.95
COMBO-17 U	44.94
UV	
GALEX 2267 Å	45.04
X-ray	
Chandra 2 keV	44.35
Chandra 5 keV	44.46

Note. [a] The full set of COMBO-17 SED data points are available in Wolf et al. (2004, 2008).

emission region in units of R_G. For J0331–2755, $L_{bol} \approx 5.7 \times 10^{45}$ erg s^{-1}, $\zeta_1 \approx 200$, $\zeta_2 \approx 900$, and $W_d \approx 1.5 \times 10^{44}$ erg s^{-1}. The ratio of the Mg II luminosity to the viscous power is then $L_{Mg\,II}/W_d \approx 0.07$. Assuming that J0331–2755 has the same Hα to Mg II line ratio as Arp 102B (∼5.0; Halpern et al. 1996), the Hα luminosity is ∼35% of the total energy available locally. Based on computations of the emission from the accretion disks of cataclysmic variables in Williams (1980), we expect that no more than 20% of the local viscous energy would be emitted as Hα. Thus, the local energy is probably insufficient to power the strong lines, and external illumination of the accretion disk appears necessary to explain the observed Mg II line luminosity even for this luminous, and likely efficiently accreting, double-peaked emitter.

The source of the external illumination is still uncertain. For the prototype double-peaked emitter Arp 102B, Chen & Halpern (1989) proposed that the outer accretion disk was illuminated by a vertical extended structure in the inner disk, such as a geometrically thick and optically thin X-ray-emitting flow produced by radiatively inefficient accretion (RIAF; e.g., Rees et al. 1982; Narayan & Yi 1994). This mechanism has also been proposed to apply to other low Eddington ratio, low-luminosity double-peaked emitters. However, recent studies have revealed that some sources are actually efficient accretors, with Eddington ratio $L/L_{Edd} \gtrsim 0.1$, a regime where RIAFs cannot exist (e.g., Lewis & Eracleous 2006; see also Strateva et al. 2008). The SED of J0331–2755 shows a big blue bump (BBB) in the UV, as well as a typical X-ray photon index and luminosity for radio-loud quasars, also indicating a relatively high-efficiency accretion flow in the central engine. In Figure 3, we show the SED of Arp 102B (Eracleous et al. 2003; Strateva et al. 2008, and references therein). Compared to J0331–2755, Arp 102B has a luminosity about 2 orders of magnitude fainter and lacks a BBB. For efficiently accreting double-peaked emitters, external photons may come from a different kind of disk-illuminating structure, for example, disk photons scattered by electrons in jets or slow outflows as suggested by Cao & Wang (2006).

Another open question regarding double-peaked emitters is their connection to the general AGN population. Observationally, except for their double-peaked and generally broader emission lines, many double-peaked emitters resemble typical AGNs (e.g., through broadband optical-to-X-ray SEDs). Despite the requirement of X-ray illumination of the disk, their X-ray properties (e.g., spectra and power output) do not differ greatly from those of single-peaked AGNs (e.g., Strateva et al. 2003, 2006), though recent study suggested enhanced X-ray emission relative to the UV/optical emission in a sample of the broadest double-peaked emitters (Strateva et al. 2008). Theoretically, all luminous AGNs are expected to have accretion disks, and Keplerian disks are capable of producing double-peaked emission lines. Although the disk parameters, such as the inclination and the ratio of the inner to outer radius, could affect the appearance of the line profile, they are not sufficient to explain why only ∼3% of AGNs are double-peaked emitters. Murray & Chiang (1997) suggested that a varying optical depth in an accretion-disk wind could determine the presence of single- or double-peaked line profiles. The underlying double-peaked lines become single-peaked due to radiative transfer in a strong radiation-driven disk wind, and therefore double-peaked emission lines are mostly existent in low-luminosity AGNs, where disk winds are weak with small optical depths. However, this model cannot explain the existence of the most luminous double-peaked emitters, including J0331–2755. Alternatively, the presence of single- or double-peaked emission lines could be related to the structure and kinematics of the broad-line region (BLR). It is commonly believed that the BLR is highly stratified. The low-ionization BLR could consist of two kinematically distinct regions: an outer region of the accretion disk and a standard kinematically hot broad-line cloud component. If in the majority of AGNs line emission from the latter component dominates, we will see single-peaked broad emission lines, while in the remaining ∼3% we see double-peaked lines from the accretion disk. However, the detailed structure of the BLR is poorly understood. It seems likely that the small fraction of double-peaked emitters among AGNs is the result of a combination of these factors, i.e., the influence of external illumination, the position and inclination of the line-emitting region of the accretion disk, the presence of disk winds, and the complex geometric nature of the BLR.

The properties of J0331–2755 indicate that at higher redshift, double-peaked emitters still possess typical AGN SEDs and X-ray spectra, and the double-peaked line profile can also be explained by the Keplerian disk model.

Long-term profile variability has been found to be an ubiquitous property of double-peaked emitters (e.g., Gezari et al. 2007). As the E-CDF-S field will continue to be surveyed in spectroscopic campaigns, it is likely that additional optical/near-IR spectroscopic data for J0331–2755 can be obtained in the future. These will help to study line-profile variability and constrain better the structure and kinematics of the accretion disk, which could shed light on some of the unresolved problems discussed above.

We acknowledge financial support from NASA LTSA grant NAG5-13035 (B.L., W.N.B.), CXC grant SP8-9003A/B (B.L., W.N.B., F.E.B.), the Polányi Program of NKTH (G.S.), and the Italian Space Agency (contracts ASI–INAF I/023/05/0 and ASI I/088/06/0) and PRIN–MIUR grant 2006-02-5203 (C.V.). We thank M. Brusa, M. Eracleous, B. P. Miller, J. Wu, and Y. Xue for helpful discussions. We also thank the referee for carefully reviewing the manuscript and providing helpful comments.

REFERENCES

Arnaud, K. A. 1996, in ASP Conf. Ser. 101, Astronomical Data Analysis Software and Systems V, ed. G. H. Jacoby & J. Barnes (San Francisco, CA: ASP), 17
Broos, P., et al. 2000, User's Guide for the TARA Package (Univ. Park: Pennsylvania Sate Univ.)
Caldwell, J. A. R., et al. 2008, ApJS, 174, 136
Cao, X., & Wang, T.-G. 2006, ApJ, 652, 112
Chen, K., & Halpern, J. P. 1989, ApJ, 344, 115
Chen, K., Halpern, J. P., & Filippenko, A. V. 1989, ApJ, 339, 742
Elvis, M., et al. 1994, ApJS, 95, 1
Eracleous, M., & Halpern, J. P. 1994, ApJS, 90, 1
Eracleous, M., & Halpern, J. P. 2003, ApJ, 599, 886
Eracleous, M., Halpern, J. P., & Charlton, J. C. 2003, ApJ, 582, 633
Eracleous, M., Halpern, J. P., Storchi-Bergmann, T., Filippenko, A. V., Wilson, A. S., & Livio, M. 2004, in IAU Symp. 222, The Interplay Among Black Holes, Stars and ISM in Galactic Nuclei, ed. T. Storchi-Bergmann, L. C. Ho, & H. R. Schmitt (Dordrecht: Kluwer), 29
Eracleous, M., Livio, M., Halpern, J. P., & Storchi-Bergmann, T. 1995, ApJ, 438, 610
Faber, S. M., et al. 2003, Proc. SPIE, 4841, 1657
Ganguly, R., Brotherton, M. S., Cales, S., Scoggins, B., Shang, Z., & Vestergaard, M. 2007, ApJ, 665, 990
Gezari, S., Halpern, J. P., & Eracleous, M. 2007, ApJS, 169, 167
Giavalisco, M., et al. 2004, ApJ, 600, L93
Gil de Paz, A., et al. 2007, ApJS, 173, 185
Halpern, J. P., Eracleous, M., Filippenko, A. V., & Chen, K. 1996, ApJ, 464, 704
Kellermann, K. I., Fomalont, E. B., Mainieri, V., Padovani, P., Rosati, P., Shaver, P., Tozzi, P., & Miller, N. 2008, ApJS, 179, 71
Kellermann, K. I., Sramek, R., Schmidt, M., Shaffer, D. B., & Green, R. 1989, AJ, 98, 1195
Lehmer, B. D., et al. 2005, ApJS, 161, 21
Lewis, K. T., & Eracleous, M. 2006, ApJ, 642, 711
Miller, N. A., Fomalont, E. B., Kellermann, K. I., Mainieri, V., Norman, C., Padovani, P., Rosati, P., & Tozzi, P. 2008, ApJS, 179, 114
Murray, N., & Chiang, J. 1997, ApJ, 474, 91
Narayan, R., & Yi, I. 1994, ApJ, 428, L13
Oke, J. B. 1987, in Superluminal Radio Sources, ed. J. A. Zensus & T. J. Pearson (Cambridge: Cambridge Univ. Press), 267
Rees, M. J., Begelman, M. C., Blandford, R. D., & Phinney, E. S. 1982, Nature, 295, 17
Reeves, J. N., Turner, M. J. L., Ohashi, T., & Kii, T. 1997, MNRAS, 292, 468
Richards, G. T., et al. 2006, ApJS, 166, 470
Rovilos, E., Georgakakis, A., Georgantopoulos, I., Afonso, J., Koekemoer, A. M., Mobasher, B., & Goudis, C. 2007, A&A, 466, 119
Stark, A. A., Gammie, C. F., Wilson, R. W., Bally, J., Linke, R. A., Heiles, C., & Hurwitz, M. 1992, ApJS, 79, 77
Steffen, A. T., Strateva, I., Brandt, W. N., Alexander, D. M., Koekemoer, A. M., Lehmer, B. D., Schneider, D. P., & Vignali, C. 2006, AJ, 131, 2826
Strateva, I. V., Brandt, W. N., Eracleous, M., & Garmire, G. 2008, ApJ, 687, 869
Strateva, I. V., Brandt, W. N., Eracleous, M., Schneider, D. P., & Chartas, G. 2006, ApJ, 651, 749
Strateva, I. V., et al. 2003, AJ, 126, 1720
Vanden Berk, D. E., et al. 2001, AJ, 122, 549
Vestergaard, M., & Wilkes, B. J. 2001, ApJS, 134, 1
Williams, R. E. 1980, ApJ, 235, 939
Wills, B. J., Netzer, H., & Wills, D. 1985, ApJ, 288, 94
Wolf, C., Hildebrandt, H., Taylor, E. N., & Meisenheimer, K. 2008, A&A, 492, 933
Wolf, C., et al. 2004, A&A, 421, 913